Nanoscale

PAPER

Microwave-hydrothermal synthesis and characterization of nanostructured copper substituted ZnM_2O_4 (M = Al, Ga) spinels as precursors for thermally stable Cu catalysts†

Franziska Conrad,[a] Cyriac Massue,[bc] Stefanie Kühl,[b] Edward Kunkes,[b] Frank Girgsdies,[b] Igor Kasatkin,[b] Bingsen Zhang,[b] Matthias Friedrich,[d] Yuan Luo,[d] Marc Armbrüster,[d] Greta R. Patzke*[a] and Malte Behrens*[b]

Nanostructured $Cu_xZn_{1-x}Al_2O_4$ with a Cu : Zn ratio of ¼ : ¾ has been prepared by a microwave-assisted hydrothermal synthesis at 150 °C and used as a precursor for $Cu/ZnO/Al_2O_3$-based catalysts. The spinel nanoparticles exhibit an average size of approximately 5 nm and a high specific surface area (above 250 $m^2\,g^{-1}$). Cu nanoparticles of an average size of 3.3 nm can be formed by reduction of the spinel precursor in hydrogen and the accessible metallic Cu(0) surface area of the reduced catalyst was 8 $m^2\,g^{-1}$. The catalytic performance of the material in CO_2 hydrogenation and methanol steam reforming was compared with conventionally prepared $Cu/ZnO/Al_2O_3$ reference catalysts. The observed lower performance of the spinel-based samples is attributed to a lack of synergetic interaction of the Cu nanoparticles with ZnO due to the incorporation of Zn^{2+} in the stable spinel lattice. Despite its lower performance, however, the nanostructured nature of the spinel catalyst was stable after thermal treatment up to 500 °C in contrast to other Cu-based catalysts. Furthermore, a large fraction of the re-oxidized copper migrates back into the spinel upon calcination of the reduced catalyst, thereby enabling a regeneration of sintered catalysts after prolonged usage at high temperatures. Similarly prepared samples with Ga instead of Al exhibit a more crystalline catalyst with a spinel particle size around 20 nm. The slightly decreased Cu(0) surface area of 3.2 $m^2\,g^{-1}$ due to less copper incorporation is not a significant drawback for the methanol steam reforming.

1. Introduction

The design and understanding of heterogeneous catalysts is a topic of urgent research interest for the synthesis of basic chemicals as well as for sustainable energy strategies. Catalytic methanol synthesis, for example, is a mature industrial process with a worldwide demand of *ca.* 40 megatons per year.[1] Syngas mixtures ($CO/CO_2/H_2$) are converted over $Cu/ZnO/Al_2O_3$ catalysts formally according to

$$CO_2 + 3H_2 \rightarrow CH_3OH + H_2O. \quad (1)$$
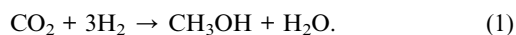
[a] Institute of Inorganic Chemistry, University of Zurich, CH-8057 Zurich, Switzerland. E-mail: greta.patzke@aci.uzh.ch; Fax: +41 44 635 6802; Tel: +41 44 635 4691

*[b] Fritz Haber Institute of Max Planck Society, Department of Inorganic Chemistry, Faradayweg 4-6, 14195 Berlin, Germany*

[c] Ecole Polytechnique Paris Tech, Route de Saclay, 91128 Palaiseau Cedex, France

[d] Max-Planck-Institut für Chemische Physik fester Stoffe, Nöthnitzer Strasse 40, 01187 Dresden, Germany

† Electronic supplementary information (ESI) available: More experimental details with further SEM, XRD, BET and TEM data. See DOI: 10.1039/c2nr11804a

Despite the long period of industrial application of over 40 years, the underlying reaction mechanism is still discussed in the current literature.[2] Nowadays, CO_2 is generally accepted as the main carbon source of methanol from syngas as proven by isotope labeling experiments.[2,3]

This has aroused intense research interest in the structure and reactivity of this catalytic system and related materials. Recent investigations are inspired from the potential of the methanol synthesis reaction for the chemical fixation of the greenhouse gas CO_2 and the potential use of methanol as a synthetic fuel or as a hydrogen storage molecule.[4] Hydrogen can be liberated from methanol *via* the methanol steam reforming (MSR) reaction, formally the reverse reaction of (1):

$$CH_3OH + H_2O \rightarrow CO_2 + 3H_2. \quad (2)$$
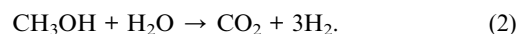
Cu-based catalysts are active both in methanol synthesis as well as in methanol steam reforming.[5] Furthermore, they are also used in water gas shift reaction[6] and for the synthesis of higher alcohols.[7] Commercial catalysts are highly optimized for the synthesis of methanol under industrial conditions (CO-containing syngas, 50–100 bars, 200–300 °C). For application in CO_2 hydrogenation, *i.e.* in feed gas mixtures without CO, the

selectivity of the catalysts needs improvement, because reaction (1) is coupled with the reverse water gas shift reaction (rWGS):

$$CO_2 + H_2 \rightarrow CO + H_2O, \qquad (3)$$
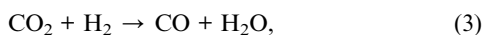
which yields significant amounts of undesired CO. For the MSR reaction, higher stability and selectivity towards CO_2 are mandatory.[8] Therefore, the influence of the preparative strategy on the final catalyst properties has to be known in detail.

Industrial $Cu/ZnO/Al_2O_3$ catalyst synthesis is a complex multi-step process[9] that depends on the controlled segregation of CuO and ZnO from a homogeneous hydroxycarbonate precursor, followed by the reduction of the resulting CuO nanoparticles to accessible Cu catalyst centers.[10] Different mixed Cu/Zn-precursor phases lead to various catalyst microstructures[11] of the resulting Cu/ZnO composites which again differ with respect to particle sizes, crystallinity, Cu lattice strain and particle embedment. These properties have been shown to affect the intrinsic activity of the exposed Cu surface probably by metal–oxide interactions.[12] This is a major driving force for exploring novel precursor compounds with a mixed cationic lattice of Cu^{2+}, Zn^{2+} and Al^{3+} to find $Cu/ZnO/Al_2O_3$ related catalysts with new microstructures and superior catalytic properties in CO_2 hydrogenation or MSR.

In this context, the spinel-type oxide $A^{II}B^{III}_2O_4$ (A = Cu, Zn; B = Al) is an attractive oxide matrix due to its high thermal stability and mechanical resistance together with the advantage of hosting all three relevant metal species in a mixed cation lattice. This is a good prerequisite for the required homogeneous distribution of Cu^{2+} ions in the precursor prior to their reduction to small Cu nanoparticles with an intimate interface contact to the redox-inert oxide matrix. $ZnAl_2O_4$ has already attracted interest as a support for Cu-based methanol synthesis catalysts[13] and $ZnAl_2O_4{:}Cu^{2+}$ materials are furthermore useful for the selective reduction of NO_x as well as for methane combustion.[14]

Spinels have traditionally been accessed by ceramic high temperature methods with the drawback of low surface areas. While conventional $Cu/ZnO/Al_2O_3$ catalyst precursor materials, such as hydroxy-carbonates, generate porosity through thermally degradable anions,[10] spinel precursors need to be directly prepared in a nanosized form with high specific surface area. Especially nanostructuring of $Cu_xZn_{1-x}Al_2O_4$ requires direct and flexible synthetic methods.

For this purpose, microwave-assisted techniques are an up-to-date approach that offers parameter control to generate materials with low particle sizes and high surface areas.[15] Microwave-solvothermal (MW-ST) synthesis of $ZnAl_2O_4$ and its Pt- and Pd-loaded forms as well as the microwave-hydrothermal (MW-HT) synthesis of pristine $ZnAl_2O_4$ have been described,[16] and $ZnAl_2O_4/CuO$ composites as catalysts for o-alkylation of phenol have been obtained with conventional hydrothermal strategies.[17] Only recently $ZnAl_2O_4/CuO$ catalysts have been accessed for soot oxidation with a microwave-glycothermal route.[18] Furthermore, microwave treatment of $CuO/ZnO/Al_2O_3$ obtained from conventional co-precipitation has been shown to have a beneficial effect on the MSR activity of the resulting $Cu/ZnO/Al_2O_3$ catalysts after reduction.[19] This effect has been attributed to increased strain in the Cu particles.

However, the effect of MW-HT treatment on the materials properties and catalytic performance of $Cu/ZnO/Al_2O_3$ catalysts has never been investigated. Some of the authors have recently developed a new MW-HT approach for the production of otherwise elusive nanostructured $ZnGa_2O_4{:}Cu^{2+}$ materials that permits adjustment of their copper content in a single reaction step from metal sulfates and chlorides.[20]

In this study, we report on the application of this approach for the preparation of $Cu/ZnO/Al_2O_3$ related catalysts from $Cu_xZn_{(1-x)}Al_2O_4$ spinel precursors. We have tested the resulting material in CO_2 hydrogenation and MSR in comparison with conventionally prepared $Cu/ZnO/Al_2O_3$ reference catalysts. Furthermore, we present complementary catalytic and synthetic studies on Ga-containing spinel analogues.[20] Generally, gallium oxides leave room for interesting explorations as an emerging class of tunable catalysts. Ga_2O_3, for example, has been used as a promoter for Cu/ZnO catalysts[21] and it was recently shown to significantly improve the stability of the catalyst in the hydrogenolysis of glycerol.[22] $CuGa_2O_4$ catalyzes the steam reforming of dimethyl ether.[23] Furthermore, mixed Ga_2O_3/Al_2O_3 catalysts have high tuning potential, e.g. for the selective catalytic reduction of NO[24] or steam reforming of dimethyl ether.[25] As metal–oxide interactions are crucial for the accessibility of embedded Cu catalyst centers, further investigations on Cu-containing gallium spinels are now required to understand the influence of various M^{III} cations on the catalytic performance of spinel hosts.

In the following, we compare ZnM_2O_4/CuO (M = Al, Ga) spinels with respect to their MW-HT assisted synthesis and the redox behaviour of the emerging nanoscale catalyst precursors. The properties of the obtained Cu-containing catalysts are compared to commercial standards, and new perspectives for tuning spinel-derived $Cu/ZnO/M_2O_3$ (M = Al, Ga) catalysts are discussed.

2. Experimental section

2.1. Microwave-hydrothermal (MW-HT) synthesis

Zinc nitrate ($Zn(NO_3)_2 \cdot 6H_2O$, Sigma-Aldrich, $\geq$99%), copper nitrate ($Cu(NO_3)_2 \cdot 3H_2O$, Carl Roth, $\geq$99%) and aluminium nitrate ($Al(NO_3)_3 \cdot 9H_2O$, Sigma-Aldrich, $\geq$98.5%) were used without further purification and dissolved in micropore Q+ water with a nominal Cu : Zn : Al ratio of ¼ : ¾ : 2. Aqueous ammonia solution (Merck, 25%) or freshly prepared 2 M NaOH solution was used as a precipitating agent. The basic precipitating agent was added to the magnetically stirred solution manually drop-by-drop until the desired pH was stable. 50 mL of the obtained suspension were immediately transferred into a microwave Teflon vessel (DAP-80+) for MW treatment. The suspension was heated within 30 min up to 150 °C in a speedwave MWS-3 + Microwave Digestion System (Berghof) at 2.45 GHz and 1450 W. The reaction temperature was kept constant for 1 or 2 h, followed by a 30 min cooling period. After cooling, all products were washed with deionized water, vacuum filtered and dried in air at 80 °C for 2 h. Samples are labeled as follows: Metal_[pH value]_base_[time in h]. An overview of the $Cu_xZn_{1-x}M_2O_4$ (M = Al, Ga) samples prepared with the MW method is given in Table 1.

Table 1 Overview of the $Cu_xZn_{1-x}M_2O_4$ (M = Al, Ga) catalyst precursors prepared with a nominal Cu : Zn ratio of ¼ : ¾ at 150 °C

Sample	FHI-DB#[a]	Precipitating agent	pH[b]	MW-time/h
Al_7.5_NH3_1	9735	NH_3	7	1
Al_9_NH3_1	9671	NH_3	9	1
Al_9.5_NH3_1	9674	NH_3	9.5	1
Al_9_NaOH_1	9742	NaOH	9	1
Al_10_NaOH_1	9770	NaOH	10	1
Al_10_NaOH_2	9828	NaOH	10	2
Al_10.5_NaOH_1	9771	NaOH	10.5	1
Al_11_NaOH_2	9830	NaOH	11	2
Al_11.5_NaOH_2	9831	NaOH	11.5	2
Ga_10.5_NH3_1	10 016	NH_3	10.5	1

[a] Sample number in FHI-AC database (http://reload.rz-berlin.mpg.de/sndb/adm.epl?mode=login). [b] Initial pH of suspension before MW treatment.

$Cu_xZn_{1-x}Ga_2O_4$ was synthesized according to ref. 20 and the composition corresponds to the sample designated as ZnCuGa_4 therein (for experimental details see ESI†). Twenty identical samples were assembled for catalytic MSR tests.

2.2. Analytical characterizations

X-Ray diffraction (XRD) measurements were performed on a STOE STADI P transmission diffractometer equipped with a primary focusing germanium monochromator (Cu $K_{\alpha 1}$ radiation) and a linear position sensitive detector. Small amounts of powder were sandwiched between two layers of polyacetate film and fixed with a small amount of X-ray amorphous grease (Al-containing samples) or between adhesive tape (Ga-containing samples). In the former case, the signal appearing near $2\theta = 18°$ in some of the XRD-patterns is caused by the grease used to fix the powder at the sample holder.

In situ XRD of the reduction of sample Al_10_NaOH_1 was performed in two consecutive heating–cooling cycles with the same temperature programs. In order to distinguish between the effects of sintering and reduction of the material, the first (sintering) cycle was conducted in artificial air (20% O_2 in He), while the second (reduction) cycle was performed in 5% H_2 in He. Before and after each temperature treatment, the sample was characterized with an XRD scan at 25 °C (13–67° 2θ in steps of 0.02°, 2 seconds per step). The temperature cycles were performed with ramp rates of 20 K min^{-1} and isothermal holding segments every 50 °C from 50 to 500 and back to 50 °C. Each holding segment consisted of a waiting time of 5 minutes followed by an XRD scan (25–50° 2θ in steps of 0.02°, 2 seconds per step), totaling to about 55 minutes per hold.

A similar strategy was pursued for the investigation of Ga_10.5_NH3_1 with *in situ* XRD. Two identical consecutive heating–cooling cycles were performed, the first in He, the second in 5% H_2 in He. Before and after each cycle, a long XRD scan (10–100° 2θ in steps of 0.02°, 15 seconds per step) was performed at 25 °C. For the temperature programs, heating/cooling rates of 20 K min^{-1} were employed. Isothermal holding segments with a waiting time of 5 minutes and two fast XRD scans (13–67° 2θ in steps of 0.02°, 2 seconds per step) were performed every 50 °C in the range 100–400–100 °C (225 minutes per hold). As no irreversible changes of the lattice parameters were observed for the

reduction cycle, a third cycle in 5% H_2 in He was conducted in the temperature range 400–600–400 °C.

Furthermore, the cation composition was investigated with X-ray fluorescence (XRF) measurements and LA-ICP-MS methods. XRF measurements were performed in He atmosphere on a wavelength-dispersive Sequential Pioneer S4 Spectrometer (Bruker) using the powder samples and the K lines of Cu and Zn were analyzed. LA-ICP-MS analyses of the pressed powder samples were carried out using a 193 nm ArF excimer laser ablation system (Lambda Physik) coupled to an ICP-MS (DRC II +, Perkin–Elmer). Samples were ablated for 40 s (5 Hz, 60 μm crater diameter) and the operating conditions are summarized in Table S1†.

The morphology of the samples was characterized with scanning electron microscopy on a LEO 1530 (FEG); samples were dispersed in ethanol and applied on a silicon wafer. SEM/EDX investigations were carried out on a Hitachi S-4800 (FEG) system.

A Philips CM200FEG microscope operated at 200 kV and equipped with a field emission gun, Gatan imaging filter and energy-dispersive X-ray (EDX) analyzer was used for TEM investigations. The coefficient of spherical aberration was $C_s = 1.35$ mm and the information limit better than 0.18 nm. High-resolution images were taken at a magnification of 1 083 000× with a CCD camera and selected areas were processed to obtain the power spectra (square of the Fourier transform of the image), which were used for measuring interplanar distances (±0.5%) and angles (±0.5°) for phase identification.

Static nitrogen physisorption experiments of the Al-containing samples were performed in an Autosorb-1C setup (Quantachrome). Prior to the measurements, the samples were degassed for 2 h under dynamic vacuum at 80 °C. The data were analyzed according to the BET theory using the multipoint method (11 points). The specific surface area of the Ga-containing samples was investigated with a Quadrasorb *SI* (Quantachrome) by degassing at 150 °C for 2 h and applying a 5 point BET determination.

Samples for UV/vis spectroscopy were well ground and filled between two precision quartz object holders with a definite light path of 0.1 mm. Spectra were recorded in the 200 to 800 nm range on a Perkin Elmer Lambda 650 spectrometer with an integrating sphere setup (diameter 150 mm).

For temperature programmed reduction (TPR) measurements, the material was reduced (5% H_2/Ar, 80 ml min^{-1}, 6 K min^{-1}) in a fixed bed reactor (CE instruments TPDRO-1100). H_2 consumption was monitored with a thermal conductivity detector. The copper surface area was determined in the same setup using N_2O reactive frontal chromatography (RFC) by monitoring the amount of evolved N_2 upon decomposition of N_2O at the Cu(0) surface at room temperature, which was quantified from the time interval of the frontal chromatogram of N_2 recorded at defined flow by mass spectrometry (*i.e.* the time interval between the onset of the N_2 peak and the detection of N_2O).[26] For calculation of the copper surface area, a stoichiometry of $Cu/N_2 = 2$ and a value of 1.46×10^{19} Cu atoms m^{-2} were used.[27]

2.3. Catalytic tests

Catalytic tests in CO_2 hydrogenation were carried out in a standard fixed bed, high pressure down-flow methanol synthesis

reactor coupled to an Agilent 7890A Gas Chromatograph (GC). 1 g of the catalyst precursor was mixed with inert silica (Fluka Silica Gel 60). The mixture was loaded into the reactor and first reduced in 100% H_2. The temperature was raised to 300 °C with a 2 K min^{-1} rate using a 100 cm^3 min^{-1} gas flow and held constant at 300 °C for 90 min. The catalytic activity of the reduced catalyst was afterwards tested in the same reactor with a gas mixture of 24% CO_2, 72% H_2, and 4% Ar (200 cm^3 min^{-1}; $p = 50$ bar) at 220 °C for 2 h and at 250 °C for another 2 h. Identical conditions were applied for the testing of the commercial $Cu/ZnO/Al_2O_3$ catalyst, except that 0.2 g of catalyst were loaded into the reactor.

Methanol steam reforming (MSR) tests were carried out in a silica-coated stainless steel plug-flow reactor system. A sieve fraction of 100–200 μm (125 mg Al_10.5_NaOH_2 and 500 mg Ga_10.5_NH3_1 catalyst) was diluted with 200 mg of inert graphite each. Before starting the steam reforming reaction both catalysts were reduced in hydrogen (10% H_2 in N_2, 6 K min^{-1} to 300 °C for 5 h), then cooled to 260 °C with 6 K min^{-1} in He/N_2. N_2 was used as a carrier gas and He as a tracer gas. The gas flow was switched to $MeOH/H_2O$ (1 : 1) to run the MSR reaction at 260 °C for 20 h. The flow of the $MeOH/H_2O$ mixture was 0.01 cm^3 min^{-1}. The products were analyzed by GC (CP 4900, Varian, Columns: Molsieve, PPU). The gas volumes were calibrated by the He tracer. One out of three GC columns was run on argon as carrier gas to quantify the He tracer concentration. Unconverted water and methanol were removed prior to the GC using a cooling trap and a Nafion membrane with counter-flowing nitrogen at 90 cm^3 min^{-1}. Selectivity of CO_2 was defined as $CO_2/(CO_2 + CO)$.

For both reactions conventionally prepared $Cu/ZnO/Al_2O_3$ catalysts[9b,28] were used as reference and tested under the same conditions. Detailed characterizations of this material are provided in previous studies.[10,12b,29]

3. Results and discussion

First, we focus on the influence of the MW-HT parameters on composition, morphology and surface area of the spinel materials. Next, we compare the thermal redox behavior of the different spinel types, followed by a discussion of their catalytic performance in methanol synthesis by CO_2 hydrogenation and methanol steam reforming.

3.1. MW-HT synthesis and characterization of $Cu_{1-x}Zn_xAl_2O_4$

The materials obtained in the Cu–Zn–Al system generally exhibit only weak and broad reflections in their XRD patterns indicative of poor crystallinity and/or small crystallite sizes (Fig. 1). Background modulations are detected near positions where strong lines of the $ZnAl_2O_4$ spinel are expected. The sample obtained with NaOH as precipitating agent shows a slightly better crystallinity. The absence of well-defined peaks prevents the analysis of the cationic composition of the material by XRD, which is generally difficult due to the closely related scattering factors of Cu and Zn, the similar ionic radii of Cu^{2+} and Zn^{2+}, and the effect of the cation distribution on the lattice parameter of the spinel.[30] The question whether copper was effectively
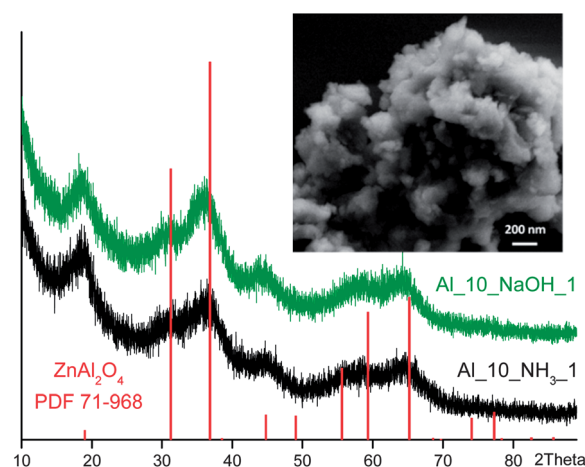

Fig. 1 Representative XRD patterns of the $Cu_xZn_{1-x}Al_2O_4$ spinel phase obtained by MW-HT treatment of Cu-, Zn- and Al-nitrates precipitated at pH 10 with NH_3 (Al_10_NH3_1) and NaOH (Al_10_NaOH_1). The inset shows a representative SEM image of Al_10_NaOH_1.

incorporated into the spinel phase was addressed using a combination of integral and local chemical analysis (see below).

Variation of synthesis parameters, which is described in detail in the ESI†, has shown that the pH value of the initial suspension is a key parameter for spinel formation. The XRD patterns of the sample obtained from the pH variation experiments are shown in Fig. S1†. The pH window for spinel formation is rather narrow and depends on the precipitating agent (NH_3 or NaOH). The optimal values are pH 9 with NH_3 and pH 10 with NaOH. With NH_3 as a precipitating agent initial pH values above 9 favor the formation of aluminium oxide hydroxide (boehmite) (Fig. S1d†). Therefore, the presence of side products cannot be completely excluded (*cf.* UV/vis spectra in Fig. 4). Poorly crystalline CuO is formed if NaOH is used at pH >10 (Fig. S1d†). Prolonging the reaction time to 2 h was found to reduce the formation of unwanted CuO particles (Fig. S2† and Section 3.3.). On the other hand, hydrotalcite-type compounds with nitrate anions are formed if the pH is further lowered (Fig. S1a and c†). Although mixed Cu, Zn, Al hydrotalcites have been shown to be suitable precursor materials for Cu-based catalysts in a number of reports,[11b,31] they are not further considered in the present study that aims at the potential of mixed spinels as precursor compounds. Furthermore, SEM-EDX investigations have shown that the hydrotalcite-containing samples obtained here did not show the desired homogeneous distribution of the metal species (Fig. S3b†).

Electron microscopy reveals the presence of hierarchically arranged particles with sizes below 10 nm as can be seen in the inset of Fig. 1. HRTEM shows that the very broad width of the XRD peaks can be attributed to small crystalline domain sizes. Fig. 2a and b show representative images of the samples Al_10_NaOH_1 and Al_9_NH3_1 with crystallite sizes around 5 nm. The lattice fringes could be assigned to the spinel structure (Fig. 2a and b, insets). Judging from the HRTEM micrographs, the material was not completely crystallized after the MW treatment, and the amount of amorphous material was estimated to be higher for the sample obtained with NH_3 as a precipitating agent in agreement with the XRD analysis.
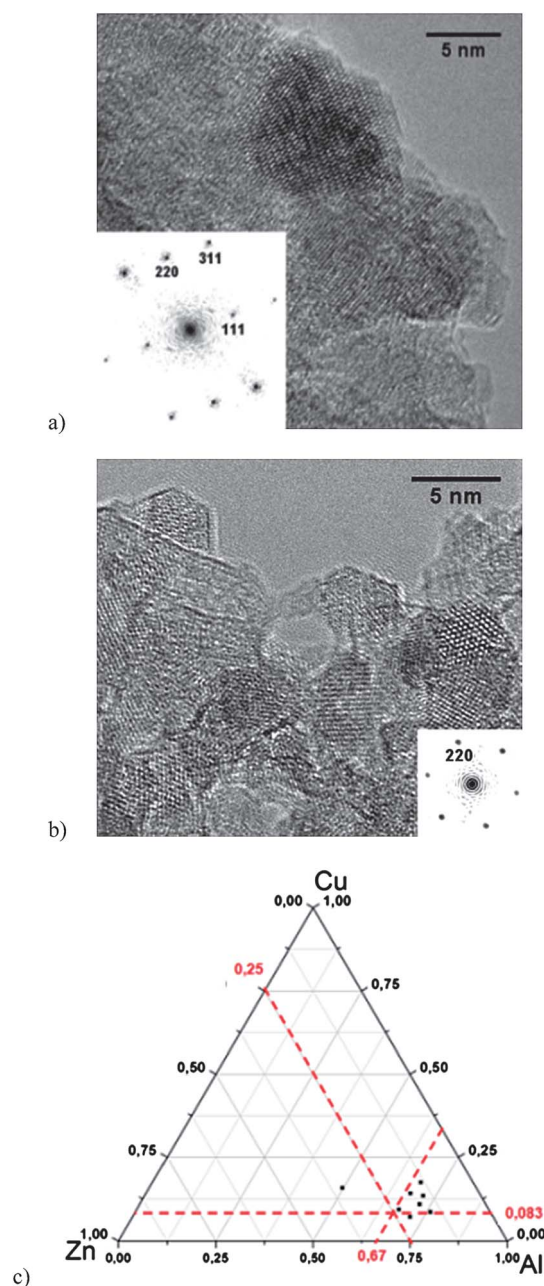
a)

b)

c)

Fig. 2 Representative electron microscopy images of $Cu_xZn_{1-x}Al_2O_4$ prepared under MW-HT conditions: HRTEM micrographs of the spinel particles (a) in Al_9_NH3_1 (zone axis [211]), (b) in Al_10_NaOH_1 (zone axis [111]), and (c) local elemental composition of Al_10_NaOH_1 determined at different locations by TEM-EDX. The red lines indicate the nominal composition.

Thermogravimetric measurements of Al_10_NaOH_1 display a considerable mass loss of 28% up to 500 °C (Fig. S4 and S5†) which is attributed to desorption of water molecules (94 °C, *ca.* 11%) and decomposition of OH groups tentatively located in the amorphous domains of the as-prepared material (247 °C, *ca.* 17%). Assuming that the amorphous domains consist of hydroxides, the fraction of uncrystallized material can be estimated on the basis of TGA results to approximately 50% in the as-prepared sample. Accordingly, calcination at 800 °C leads to

a significant intensity increase of the characteristic spinel reflections in the XRD pattern (Fig. S4†). The residue obtained after heating to 1400 °C under N_2 atmosphere displays a distinct spinel pattern with pronounced and sharp high intensity reflections.

Local EDX analyses of the as-prepared materials revealed that all elements are relatively homogeneously distributed in the material, thus serving as an additional indicator that Cu is incorporated into the $ZnAl_2O_4$ spinel. In general, the local Cu : Zn ratios determined *via* EDX (Fig. 2c and S3a–e†) did not show large deviations from the integral composition determined by XRF (Table 2). Highly precise LA-ICP-MS measurements, however, reveal a slight excess of Cu.

In the case of the sample prepared with NH_3, the Cu : Zn ratio after the synthesis was significantly below the nominal value of 25 : 75 (Table 2), thereby indicating a loss of copper during MW-HT treatment. This can be explained with the formation of soluble blue copper ammine complexes, which prevent a significant fraction of the Cu from precipitation and colorize the supernatant solution. In comparison to MW-HT reactions in NH_3 media, the use of NaOH improves the degree of copper incorporation and affords a Cu : Zn ratio of the products, which is closer to the composition of the starting solution (Table 2).

From the observation of spinel formation with XRD and HRTEM in combination with the absence of any segregated Cu phase and the agreement of the local, integral and nominal composition in samples prepared under optimal conditions, the successful incorporation of Cu^{2+} in the $ZnAl_2O_4$ spinel lattice and formation of a mixed spinel $Cu_{1-x}Zn_xAl_2O_4$ can be concluded.

Specific surface areas around 300 m^2 g^{-1} were determined by N_2 physisorption (Table 2, Fig. S6†). This value is very high[32] and in agreement with the nanostructured nature of the crystallites observed by XRD and TEM. The high surface area may be in part attributed to the amorphous domains of the material observed in TEM. After thermal reduction in hydrogen at 310 °C (see below), the sample Al_NaOH_10_2 still exhibits a specific surface area of 101 m^2 g^{-1}.

The analytical data in their entirety show that MW-HT methods provide a nanostructured spinel material $Cu_{1-x}Zn_xAl_2O_4$ ($x \approx 0.7$) with a homogeneous incorporation of Cu^{2+} in the host lattice together with a high surface area. NaOH solutions for pH adjustment are the medium of choice, because they promote copper incorporation and particle crystallinity in comparison with aqueous NH_3.

3.2. MW-HT parameter influence on $ZnGa_2O_4$:Cu^{2+}

The influence of microwave power and device type on the quality of the products is a well known phenomenon in microwave-assisted materials synthesis.[15c] Reference experiments on the MW-HT formation of pristine $ZnAl_2O_4$ in a different device with 1600 W microwave power (MARS 5, *cf.* Experimental section) led to spinel-type products with better crystallinity (Fig. S2†). As Cu/Ga-based spinels have proven difficult to be accessed with conventional methods, we performed Cu-incorporation experiments with $ZnGa_2O_4$ while applying higher microwave power. In the following, the emerging synthetic trends and materials properties for Zn/Ga-based spinel precursors are compared to the MW-HT synthesis of $Cu_{1-x}Zn_xAl_2O_4$ spinels.

Table 2 Chemical compositions and BET-surface areas of selected spinel samples[a]

Sample	Cu : Zn (XRF/EDX[b])	Composition[c]	BET SA/ m² g⁻¹
Al_9_NH₃_1	9 : 91/13 : 87	$Cu_{0.12}Zn_{0.88}Al_2O_4$	299
Al_10_NaOH_2	26 : 74/26 : 74	$Cu_{0.35}Zn_{0.65}Al_2O_4$	268
Al_10.5_NaOH_2	26 : 74/27 : 73	*n.m.*	279
Al_10.5_NaOH_1	*n.m.*/24 : 76	$Cu_{0.36}Zn_{0.64}Al_2O_4$	334
Ga_10.5_NH₃_1	*n.m.*	$Cu_{0.05}Zn_{0.95}Ga_2O_4$	72

[a] *n.m.* = not measured. [b] Average of 5–10 local measurements. [c] Measured with LA-ICP-MS.

Prior to the introduction of Cu into the reaction system, the influence of NaOH and NH₃ on the MW-HT formation of pristine $ZnGa_2O_4$ was investigated. Spinel formation starts around pH 8 for NaOH in comparison to higher values (pH 10) for NH₃, but the products obtained in the presence of NH₃ display a higher crystallinity (Fig. S7†). On the one hand, the use of ammonia as a complexing agent may limit the extent of copper incorporation through complexation side reactions (*cf.* above)—but on the other hand, it permits pH adjustment without the introduction of non-essential cations into the reaction mixture. Therefore, the synthesis of $ZnGa_2O_4:Cu^{2+}$ was performed in ammonia solutions: mixtures of gallium- and zinc sulfate with systematically increased amounts of copper chloride were treated for one hour at 150 °C (Fig. 3). The pH window for the formation of $ZnGa_2O_4:Cu^{2+}$ with good crystallinity is between pH 10 and 10.5. Spinel formation already sets in around pH 6, but pH values below 10 bring forward impure products of considerably lower crystallinity.[20]

Due to the lower degree of Cu incorporation, the Ga-containing systems are better described as Cu^{2+}-doped $ZnGa_2O_4$ materials, $ZnGa_2O_4:Cu^{2+}$, than as mixed spinels formed by cation substitution.

The individual particle sizes are in the range below 20 nm and thus larger than those observed for Al-containing samples. Generally, the extent of copper incorporation into nanostructured $ZnGa_2O_4$ is lower than the copper uptake of the $ZnAl_2O_4$ matrix
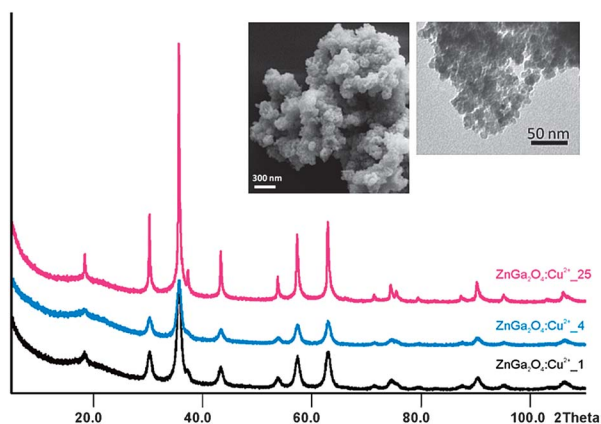
under MW-HT conditions; whereas in the latter a Cu : Zn ratio around 10 : 90 is possible, their gallium-containing analogues can host a Cu : Zn ratio of maximum 5 : 95 under optimized MW-HT preparation conditions. The distorted octahedral coordination of the Cu^{2+} centers in the $ZnGa_2O_4$ spinel lattice was confirmed with a wide range of analytical methods including EXAFS and magnetic measurements.[20]

When comparing the preparative parameters for the Ga- and Al-containing systems, it is noteworthy that the practical handling of the Al-based spinels is less facile than the workup of zinc gallates; whereas the latter can be easily filtered off and washed to generate dry powders, the colloidal and viscous nature of the $ZnAl_2O_4$ samples renders them difficult to isolate and to purify. This technical inconvenience is a side effect of their superior BET surface areas (*cf.* Table 2). In terms of MW-HT synthesis, both systems are accessible from comparably straightforward one-step protocols. The copper host matrices have individual assets and drawbacks; whereas the crystallinity of nanoscale $ZnGa_2O_4:Cu^{2+}$ is considerably higher, $ZnAl_2O_4:Cu^{2+}$ synthesis offers the opportunity of incorporating higher copper amounts into high surface area materials (*cf.* Experimental section).

UV/Vis spectra of selected spinel samples were recorded to determine the optical band gaps of the compounds (Fig. 4). As outlined above, the copper substituted $ZnAl_2O_4$ prepared with ammonia shows impurities which is evident from the two detected absorption bands in UV/Vis measurements. The broadened peak around 700 nm can be attributed to Cu^{2+} in the spinel matrix and corresponds to the light bluish green color of the materials. $Cu_{1-x}Zn_xAl_2O_4$ samples synthesized in the presence of NaOH (reaction times of 1 or 2 h), however, display identical UV/Vis spectra and their band gaps were determined around 3.2 eV (~390 nm), whereas the gallium containing catalyst exhibits a much wider band gap at 4.5 eV (245 nm).

3.3. Redox behaviour of the copper centers in $Cu_xZn_{1-x}M_2O_4$ (M = Al, Ga)

In the following, the redox behavior of copper in both matrices is compared as a selection criterion for further catalytic tests. The $Cu_xZn_{1-x}Al_2O_4$ samples Al_11_NaOH_2 and Al_10_NaOH_1 were subjected to temperature programmed reduction (TPR) up to 500 °C, and the results are shown in Fig. 5.
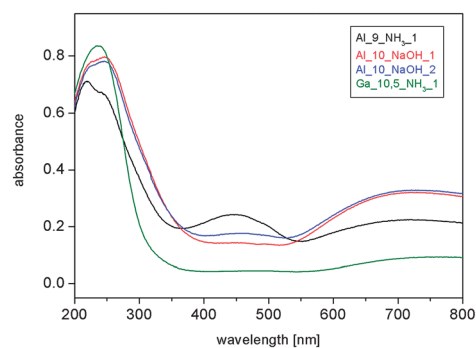

Fig. 3 Representative XRD patterns of nanostructured $ZnGa_2O_4:Cu^{2+}$ with SEM and HRTEM images (inset). The initial copper content in the starting solution is expressed as $ZnGa_2O_4:Cu^{2+}\_n$ (n = initial metal% of Cu^{2+} ions related to the sum of Zn, Ga and Cu). The blue curve corresponds to the Ga_10.5_NH₃_1 sample used in the catalytic tests.

Fig. 4 UV/Vis spectra of $Cu_{1-x}Zn_xAl_2O_4$ synthesized at different reaction conditions in comparison with $ZnGa_2O_4:Cu^{2+}$.

The TPR profile of Al_10_NaOH_1 (Fig. 5a) shows one asymmetric peak at 318 °C indicating the presence of a single Cu species. Shoulders at the low temperature side of the TPR profiles are usually observed for the reduction of nanostructured Cu(II) catalyst precursors and are attributed to the intermediate formation of Cu(I) species.[33] The relatively high reduction temperature indicates strong interaction between Cu and the oxide as expected for Cu^{2+} incorporation into the spinel lattice. The absence of other peaks indicates the homogeneous distribution of Cu^{2+}. The sample prepared at a higher pH of 11 contains segregated CuO (see Section 3.1), which is seen in the TPR profile as an additional peak at lower temperature (Fig. 5b). Given that no such peaks at lower temperature occur in the TPR profile of Al_10_NaOH_1 (Fig. 5a), the presence of even low amounts of CuO in this sample can be excluded, confirming that pH 10 is the optimal value for the synthesis of $Cu_{1-x}Zn_xAl_2O_4$. From the integral of the TPR curve and calibration with a pure CuO standard sample, the degree of Cu(II) → Cu(0) reduction in Al_10_NaOH_1 was determined as 99%.

Based on the TPR results, 310 °C was chosen as a suitable reduction temperature to mildly release the Cu component from the mixed spinel by reduction in hydrogen for 30 min. TEM investigations on accordingly synthesized samples reveal the formation of metallic Cu nanoparticles that are aggregated with spinel particles (Fig. 6a and b). A mean Cu particle diameter of

Fig. 5 TPR profiles showing the hydrogen consumption during reduction of $Cu_xZn_{1-x}Al_2O_4$ samples: (a) phase pure spinel isolated at pH 10 (Al_10_NaOH_1) and (b) CuO-containing sample synthesized at pH 11 (Al_11_NaOH_2).

3.3 ± 0.9 nm was obtained from particle statistics based on hundred particles and fitted with a log-normal distribution (Fig. 6c).

The metallic copper surface after reduction was determined by N_2O reactive frontal chromatography (RFC) to be 8.2 m^2 g^{-1}. This value is significantly lower than the accessible Cu surface area in industrial methanol synthesis catalysts, which typically ranges from 20 to 30 m^2 g^{-1} for Cu particles around 10 nm. Nevertheless, these results show that a $Cu/ZnO/Al_2O_3$ based catalyst has been prepared from the spinel precursor with very small and relatively uniform Cu particles and a clearly measureable Cu surface area. Assuming a spherical shape of the particles and bulk density of Cu, a theoretical Cu surface area of the hypothetically unsupported Cu nanoparticles can be calculated from the TEM results. Comparison with the measured Cu surface area reveals that only a fraction of approx. 32% of the Cu particles' surface is accessible to the gas phase, while 68% are covered by the oxide matrix. Thus, the particles are on average more strongly embedded into the oxide matrix than has been observed for conventionally prepared $Cu/ZnO/Al_2O_3$ catalysts.[12b] Together with the small size of the Cu nanoparticles, the embedment can be seen as a special characteristic of the microstructure of the ex-spinel $Cu/ZnO/Al_2O_3$ catalyst. We attribute both properties to the homogeneous distribution and strong interaction of Cu^{2+} in the spinel lattice of the precursor.

In order to further characterize the redox chemistry of the spinel material, the above sample was thermally reduced at 500 °C and re-examined after 11 days of storage in the reaction container under ambient conditions and after re-oxidation in 5% O_2 at 500 °C by XRD analysis (Fig. 7).

Broad reflections of the spinel phase can be seen in all XRD patterns. The improved crystallinity compared to the as-prepared state (Fig. 1) can be attributed to the crystallization of the amorphous domains observed in HRTEM (Fig. 2). HRTEM (Fig. 8) of the sample reduced at 310 °C and XRD after treatment at 500 °C indicate only a minor increase of the spinel crystallites due to sintering of the oxide. Even the Cu phase does not show any sharp and well-developed XRD peaks after reduction at a temperature as high as 500 °C (Fig. 7a), thus indicating that Cu remains nano-structured. This is remarkable, given that conventional $Cu/ZnO/Al_2O_3$ catalysts are typically very prone to sintering and as a rule of thumb should not be treated at temperatures exceeding 300 °C.[34] Cu nanoparticles are known to be oxidized in contact with oxygen and partial and full re-oxidation are expected in air at ambient temperature and by heating in oxygen, respectively. The subtle changes in the diffractograms (Fig. 7b and c) are best evaluated by subtracting the normalized patterns from that of the reduced sample and analyzing the difference pattern (Fig. 7d). The signature of metallic Cu is clearly seen confirming that Cu^{2+} from the spinel lattice was reduced. In the case of the sample stored in air the contribution of metallic Cu to the pattern is lowered indicating a partial re-oxidation of the Cu centers by air contact. Treatment in oxygen minimizes the content of metallic Cu. Attempts to refine the XRD patterns are reported in the ESI† (Fig. S8), but their significance should be dealt with caution due to the low pattern quality of the poorly crystalline and nanostructured samples. In the case of the re-oxidized sample, the fit improves if small amounts of Cu_2O are included in the refinement. This
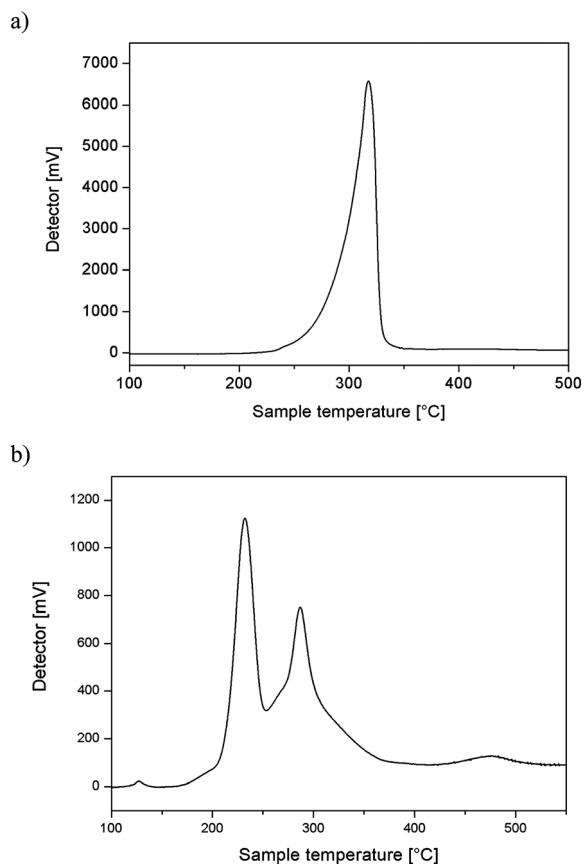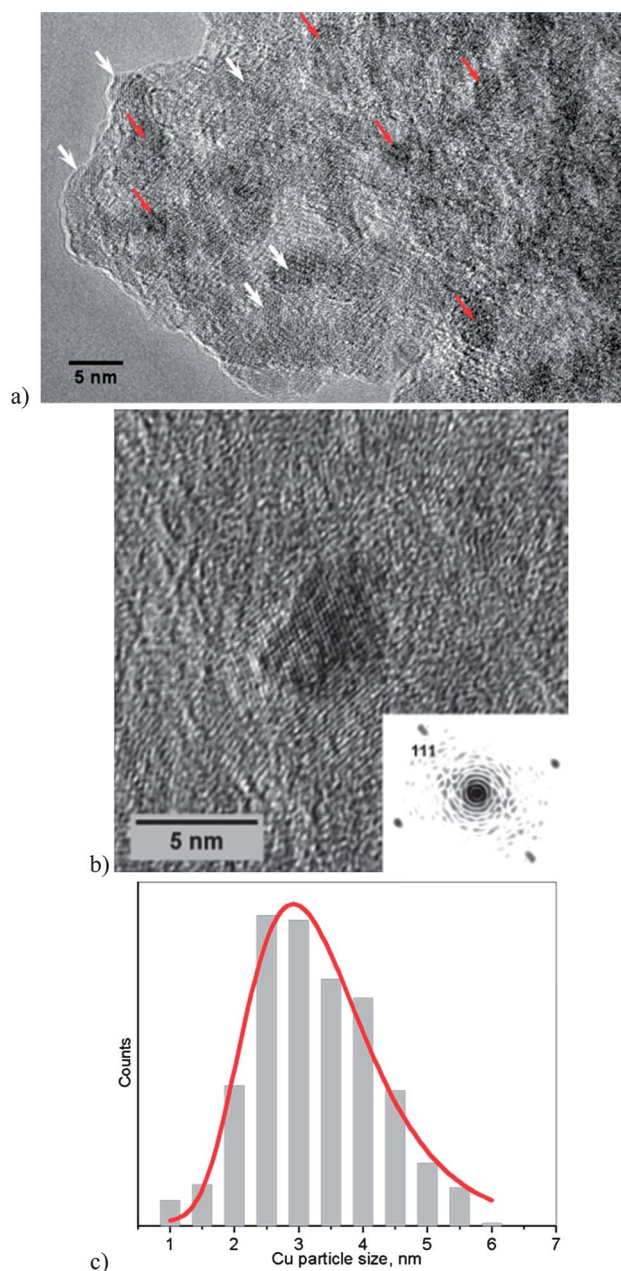
Fig. 6 (a) HRTEM image of Al_10_NaOH_1 after reductive thermal treatment in hydrogen at 310 °C (*cf.* Fig. 2a and b for pristine sample, red arrows—Cu metal, white arrows—spinel). (b) HRTEM image of an individual Cu(0) particle with power spectrum (zone axis [110]). (c) Particle size distribution of the copper nanoparticles.

result is confirmed by HRTEM investigations, which show the presence of only a few Cu_2O particles and an otherwise homogeneous Cu distribution in this sample (Fig. S9†). No crystalline CuO could be detected. On the basis of these results it is estimated that approximately 80% of the metallic Cu had been regenerated as Cu^{2+} and restored in the $Cu_xZn_{1-x}Al_2O_4$ spinel, whereas the remaining fraction of Cu had been partially oxidized to Cu_2O. This observation is in line with literature reports.[35] Thus, an at least partial oxidative regeneration of the Cu dispersion after catalyst deactivation is feasible in this system.
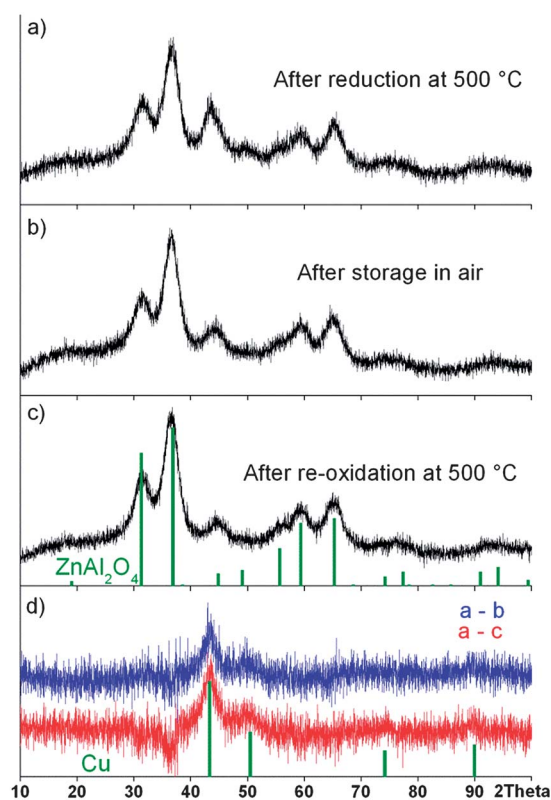

Fig. 7 XRD patterns of the $Cu_{1-x}Zn_xAl_2O_4$ sample Al_10_NaOH_1 after different pre-treatments: (a) after reduction in hydrogen at 500 °C, (b) after storage in air for 11 days, and (c) after re-oxidation in oxygen at 500 °C. Difference patterns are shown in (d). The bar graph in (c) refers to $ZnAl_2O_4$ (PDF 5-669), that in (d) to Cu (PDF 4-836).
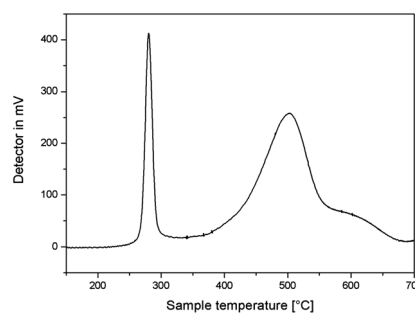

Fig. 8 TPR of nanostructured $ZnGa_2O_4$:Cu^{2+} (sample Ga_10.5_NH_3_1).

As outlined in the Experimental section, Ga_10.5_NH_3_1 was heated to 600 °C in helium atmosphere in order to distinguish possible sintering phenomena from reduction-induced effects during the *in situ* XRD experiment. This permits a clear-cut investigation of the reduction options for the incorporated copper ions with respect to catalytic applications. Neither sintering nor significant changes in the cell parameters were observed up to 400 °C and reductive thermal treatment did not change the crystallite sizes or the appearance of new diffraction peaks either. Spinel sintering sets in around 500 °C and leads to slight alterations of the unit cell dimensions that could only be detected with long-time measurements at room temperature. Although these experiments

clearly show the presence of phase pure spinel, the embedding of the Cu^{2+} species into this matrix apparently minimizes their reducibility. Related phenomena have been observed for $ZnAl_2O_4$ matrices with low degrees of copper incorporation.[18] Given that the initial copper metal content in the sample is below 5% (Table 2), the reduction process may well fall below the XRD detection limits. Nevertheless, TPR measurements (Fig. 8) display a reduction process that is obviously not reflected in a significant change of the lattice constants. Whether its initial stages involve hydrogen incorporation,[36] partial reduction of Cu^{2+} to Cu^+ or reduction of XRD-invariant surface/amorphous regions can only be speculated at this point.

TPR measurement of Ga_10.5_NH_3_1 was performed in the range from RT to 700 °C to investigate the optimal conditions for reduction experiments (Fig. 8). Two peaks were recorded: whereas the first peak at 280 °C arises from Cu^{2+} species incorporated inside the spinel structure, the second broad peak around 500 °C might be assigned to the partial reduction of Ga^{3+} in the spinel and formation of defects, e.g. oxygen vacancies. It has been shown that such defects are formed in β-Ga_2O_3, by O abstraction in reducing atmosphere at temperatures above 300 °C.[37] Ex situ XRD measurements after the reduction confirmed that the TPR treatment did not significantly change the spinel structure (Fig. S10†).

Furthermore, we performed a N_2O RFC after reduction at 300 °C and the specific copper surface area was determined to be 3.2 m^2 g^{-1}. This value is 2.5 times lower compared to the Cu(0) surface area of 8.2 m^2 g^{-1} observed for Al_10_NaOH_1. However, this was to be expected, given that the gallium containing material incorporates 2.75 times less copper in the spinel matrix than Al_10_NaOH_1. TEM investigation of the reduced sample shows that the nano-structured nature of the sample has been maintained

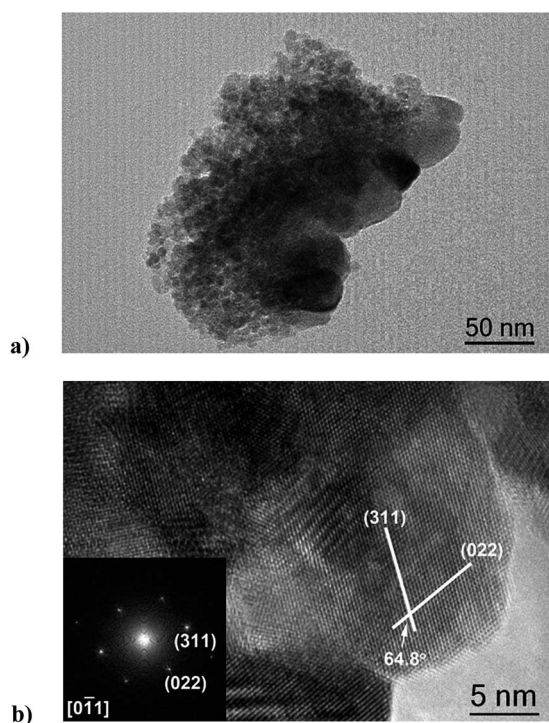**Fig. 9** Representative TEM (a) and HRTEM (b) images of the reduced $ZnGa_2O_4$:Cu^{2+} sample Ga_10.5_NH_3_1. The power spectrum refers to $ZnGa_2O_4$ (PDF 38-1240).

(Fig. 9a). Two different types of material can be detected. Larger particles on the right hand side of the aggregate are shown in Fig. 9a and smaller grains on the opposite side. A HRTEM image of an area with smaller grains is shown in Fig. 9b confirming the presence of crystalline spinel (Fig. 9b). No metallic Cu particles could be observed, probably due to their small size and their strong embedment into the spinel matrix.

3.4. Catalytic performance of $Cu_{1-x}Zn_xM_2O_4$ catalysts (M = Al, Ga)

The previously described catalyst materials were tested in CO_2 hydrogenation and methanol steam reforming (MSR). Conventionally prepared Cu/ZnO/Al_2O_3 catalysts were used as references for both reactions. A detailed characterization of this material can be found in preceding works.[10,12b,29]

Methanol synthesis tests were performed at 250 °C. An overall CO_2 conversion of 4% was observed and the selectivity for CO (85%) was considerably higher than for methanol (15%). In comparison, the conventional catalyst exhibits 9% CO_2 conversion and a methanol selectivity of 62% already at a temperature of 220 °C (Table 3), at which the spinel-based catalysts did not show any activity. The Cu surface area of the conventional catalysts was higher by a factor of ca. 3.7, but this alone cannot compensate for the differences in conversion considering the higher catalyst mass and reaction temperature of the spinel-based sample. Thus, the intrinsic activity of the exposed Cu surface of this sample is lower. Interestingly, also the selectivities of both samples differ considerably. While a large fraction of CO_2 is hydrogenated to methanol over the conventional catalyst, it is mostly converted into CO by the rWGS reaction over the spinel-based sample.

The MSR data of the catalysts after 2 and 20 h time-on-stream are summarized in Table 4. Regarding the conversions, the methanol steam reforming experiments reveal a similar picture. After a period of 20 h on stream, the relative hydrogen yield (experimental relative to the stoichiometric hydrogen yield) detected over 30 mg of the conventional reference sample decreases from 84% to 65%. On the other hand 125 mg of the reduced $Cu_{1-x}Zn_xAl_2O_4$ catalyst show a relative hydrogen yield of 45–54%. Also in this reaction, the different Cu surface areas loaded into the reactor alone cannot explain the difference in performance. Contrary to CO_2 hydrogenation, in the MSR reaction the selectivities of the two Cu–Zn–Al catalysts are almost equal and higher than 98%. 500 mg of the reduced $Cu_{1-x}Zn_xGa_2O_4$ catalyst only achieve ∼20% hydrogen yield. Furthermore, the selectivity to CO_2 is only 65–70%.

Table 3 Catalytic performance of ex-spinel and conventional Cu/ZnO/Al_2O_3 catalysts in methanol synthesis from CO_2/H_2

Parameter	Conventional	Spinel-based
Reaction temperature	220 °C	250 °C
Catalyst mass	0.2 g	1.0 g
CO_2 conversion	9%	4%
CO selectivity	38%	85%
CH_3OH selectivity	62%	15%
Yield CO[a]	3.6	12
Yield CH_3OH[a]	6.7	2.4

[a] In mg h^{-1}.

Table 4 Catalytic performance of spinel and conventional Cu/ZnO/Al$_2$O$_3$ catalysts in methanol steam reforming

Parameter	Conventional		Spinel			
			Cu$_{0.36}$Zn$_{0.64}$Al$_2$O$_4$		Cu$_{0.05}$Zn$_{0.95}$Ga$_2$O$_4$	
Catalyst mass/mg	30		125		500	
TOS	2 h	20 h	2 h	20 h	2 h	20 h
H$_2$ yield[a]	867	665	126	112	14	11
Rel. H$_2$ yield[b]	84	65	54	45	22	17
S$_{CO2}$[b]	98.1	99.2	98.4	98.3	70.6	66.7

[a] In mmol H$_2$ g^{-1} h^{-1}. [b] In %.

The lower total yield may be partly explained with the lower Cu surface area of the Ga-containing sample. The low CO$_2$ selectivity is either due to a higher activity of this sample for methanol decomposition in hydrogen and CO or for rWGS converting the MSR products H$_2$ and CO$_2$ into CO and H$_2$O. Since the main difference in the two spinel-based catalysts is the presence of Ga, and Ga$_2$O$_3$ has been reported to be active in rWGS,[37a] the latter explanation seems more likely.

In summary, catalytic activity of the spinel Cu$_{1−x}$Zn$_x$M$_2$O$_4$ (M = Al, Ga) catalysts in CO$_2$ hydrogenation and MSR could be observed. However, despite the successful nanostructuring of the spinel precursor and the significant Cu surface area that is exposed to the feed gases, the spinel-based catalysts were found to be clearly inferior compared to state-of-the-art Cu/ZnO/Al$_2$O$_3$ catalysts. This result is an example that beyond the mere presence of the elements Cu–Zn–Al, their solid-state-chemical state and microstructural arrangement critically determine the performance of a Cu/ZnO/Al$_2$O$_3$ catalyst. The often observed synergetic effect of the ZnO species[38] on the intrinsic activity of Cu is not prevailing if Zn^{2+} is incorporated into a crystalline spinel matrix. This is probably due to the limited reactivity of the ionic Zn in the spinel lattice. Incorporation into the stable spinel decreases the reducibility of Zn^{2+} and hinders strong metal support interaction with Cu, which have been observed in various Cu/ZnO materials[39] and proposed to play a role in the catalytic performance. Our results show that the lack of interaction with ZnO affects the activity as well as the selectivity of the exposed Cu surface and suggests participation of a distinct ZnO species at the active site of methanol synthesis.

4. Conclusions

A microwave-hydrothermal synthesis method, previously developed for the preparation of Cu-doped ZnGa$_2$O$_4$,[20] has been successfully optimized and applied for the preparation of a Cu$_{1−x}$Zn$_x$Al$_2$O$_4$ precursor material for a Cu/ZnO/Al$_2$O$_3$ catalyst of a unique microstructure. Under optimal synthesis conditions, the precursor material was obtained in nano-sized form with a homogeneous distribution of Cu and Zn cations in the spinel lattice and with a high specific surface area of around 300 m^2 g^{-1}. Reduction in hydrogen yields very small Cu particles (<4 nm), which are partially embedded in the oxide matrix and exhibit an exposed Cu surface area of 8 m^2 g^{-1}. Despite these promising properties, the catalytic performance of the material in

CO$_2$ hydrogenation and methanol steam reforming was found to be inferior to conventionally prepared Cu/ZnO/Al$_2$O$_3$ catalysts. These results highlight the crucial role of the microstructural arrangement of the components in a Cu/ZnO/Al$_2$O$_3$ composite catalyst on the nanoscale and clearly show that the synergetic role of ZnO for Cu-based catalysts is inhibited through Zn incorporation into a crystalline spinel host lattice.

Interestingly, these spinel-derived materials appear to have superior thermal stability, because the embedded Cu nanoparticles are less prone to sintering. Consequently, the inferior activity can probably be compensated by higher reaction temperatures, e.g. in methanol steam reforming, where conventional Cu-based catalysts strongly deactivate due to sintering and loss of active surface area. This new perspective will be investigated in a forthcoming study.

In addition, a MW-HT prepared ZnGa$_2$O$_3$:Cu^{2+} catalyst precursor was subjected to analogous reductive treatment and catalytic tests. Given that the gallium spinel matrix limits the copper uptake, the activity in MSR of the ZnGa$_2$O$_3$:Cu^{2+}-based catalyst is comparable to the copper-loaded zinc aluminium spinel, while the selectivity is influenced probably by participation of Ga centers in the catalytic reaction. As a consequence, the choice of the M^{III} cation in Cu/Zn-based spinel catalyst precursors is an influential parameter for the catalytic performance. Follow-up investigations on mixed Al/Ga-spinel matrices might shed more light on the complex interplay of copper uptake, thermal stability and selectivity among these widely tuneable catalytic hosts.

These results show how spinels—one of the most flexible and stable classes of solid materials—can be prepared in a nanostructured form allowing access to well-defined precursor materials for model composite catalysts, which have great potential to contribute to the understanding of the functionality of complex catalytic materials.

Acknowledgements

Notes and references

1 J. Hansen, Methanol Synthesis, in *Handbook of Heterogeneous Catalysis*, ed. G. Ertl, H. Knoezinger, F. Schüth and J. Weitkamp, Weily-VCH, 2nd edn, 2008, vol. 6, pp. 2920–2949.
2 J. B. Hansen and P. E. H. Nielsen, in *Handbook of Heterogenous Catalysis*, ed. G. Ert, H. Knötzinger, F. Schüth and J. Weitkamp, Weily-VCH, 2008.
3 G. C. Chinchen, P. J. Denny, D. G. Parker, M. S. Spencer and D. A. Whan, *Appl. Catal.*, 1987, **30**, 333.

4 (*a*) G. A. Olah, A. Goeppert and G. K. S. Prakash, *Beyond Oil and Gas: The Methanol Economy*; Wiley-VCH: Weinheim an der Bergstrasse, Germany, 2006; (*b*) M. Saito, *Catal. Surv. Jpn.*, 1998, **2**, 175; (*c*) R. Schlögl, *ChemSusChem*, 2010, **3**, 209.

5 P. J. de Wild and M. J. F. M. Verhaak, *Catal. Today*, 2000, **60**, 3.

6 M. Saito and K. Murata, *Catal. Surv. Asia*, 2004, **8**, 285.

7 V. R. Surisetty, A. K. Dalai and J. Kozinski, *Appl. Catal., A*, 2011, **404**, 1.

8 M. Behrens and M. Armbrüster, in *Catalysis for Alternative Energy Generation*, ed. L. Guczi, A. Erdohelyi, Springer, 2012.

9 (*a*) C. Baltes, S. Vukojevic and F. Schüth, *J. Catal.*, 2008, **258**, 334; (*b*) D. Waller, D. Stirling, F. S. Stone and M. S. Spencer, *Faraday Discuss. Chem. Soc.*, 1989, **87**, 107.

10 M. Behrens, *J. Catal.*, 2009, **267**, 24.

11 (*a*) B. L. Kniep, T. Ressler, A. Rabis, F. Girgsdies, M. Baenitz, F. Steglich and R. Schlogl, *Angew. Chem., Int. Ed.*, 2004, **43**, 112; (*b*) M. Behrens, I. Kasatkin, S. Kühl and G. Weinberg, *Chem. Mater.*, 2009, **22**, 386.

12 (*a*) M. M. Günter, T. Ressler, B. Bems, C. Büscher, T. Genger, O. Hinrichsen, M. Muhler and R. Schlögl, *Catal. Lett.*, 2001, **71**, 37; (*b*) M. Behrens, A. Furche, I. Kasatkin, A. Trunschke, W. Busser, M. Muhler, B. Kniep, R. Fischer and R. Schlogl, *ChemCatChem*, 2010, **2**, 816; (*c*) S. Kaluza, M. Behrens, N. Schiefenhövel, B. Kniep, R. Fischer, R. Schlögl and M. Muhler, *ChemCatChem*, 2011, **3**, 189.

13 T. Maniecki, P. Mierczyński, W. Maniukiewicz, D. Gebauer and W. Jozwiak, *Kinet. Catal.*, 2009, **50**, 228.

14 (*a*) C. Chauvin, J. Saussey, J.-C. Lavalley, H. Idriss, J.-P. Hindermann, A. Kiennemann, P. Chaumette and P. Courty, *J. Catal.*, 1990, **121**, 56; (*b*) C. Kienle, C. Schinzer, J. Lentmaier, O. Schaal and S. Kemmler-Sack, *Mater. Chem. Phys.*, 1997, **49**, 211.

15 (*a*) M. Rajamathi and R. Seshadri, *Curr. Opin. Solid State Mater. Sci.*, 2002, **6**, 337; (*b*) I. Bilecka and M. Niederberger, *Nanoscale*, 2010, **2**, 1358; (*c*) F. Gao, Q. Lu, X. Meng and S. Komarneni, *J. Mater. Sci.*, 2008, **43**, 2377; (*d*) K. L. Harrison and A. Manthiram, *Inorg. Chem.*, 2011, **50**, 3613.

16 W. Walerczyk, M. Zawadzki and J. Okal, *Appl. Surf. Sci.*, 2011, **257**, 2394.

17 (*a*) W. Mista, M. Zawadzki and H. Grabowska, *Res. Chem. Intermed.*, 2003, **29**, 137; (*b*) M. Zawadzki, *Solid State Sci.*, 2006, **8**, 14.

18 M. Zawadzki, W. Staszak, F. E. López-Suárez, M. J. Illán-Gómez and A. Bueno-López, *Appl. Catal., A*, 2009, **371**, 92.

19 X. R. Zhang, L. C. Wang, Y. Cao, W. L. Dai, H. Y. He and K. N. Fan, *Chem. Commun.*, 2005, 4104.

20 F. Conrad, Y. Zhou, M. Yulikov, K. Hametner, S. Weyeneth, G. Jeschke, D. Günther, J.-D. Grunwaldt and G. R. Patzke, *Eur. J. Inorg. Chem.*, 2010, **13**, 2036.

21 M. Saito, T. Fujitani, M. Takeuchi and T. Watanabe, *Appl. Catal., A*, 1996, **138**, 311.

22 A. Bienholz, R. Blume, A. Knop-Gericke, F. Girgsdies, M. Behrens and P. Claus, *J. Phys. Chem. C*, 2010, **115**, 999.

23 K. Faungnawakij, N. Shimoda, T. Fukunaga, R. Kikuchi and K. Eguchi, *Appl. Catal., A*, 2008, **341**, 139.

24 T. Nakatani, T. Watanabe, M. Takahashi, Y. Miyahara, H. Deguchi, S. Iwamoto, H. Kanai and M. Inoue, *J. Phys. Chem. A*, 2009, **113**, 7021.

25 T. Mathew, Y. Yamada, A. Ueda, H. Shioyama and T. Kobayashi, *Appl. Catal., A*, 2005, **286**, 11.

26 (*a*) O. Hinrichsen, T. Genger and M. Muhler, *Chem. Eng. Technol.*, 2000, **23**, 956; (*b*) G. C. Chinchen, C. M. Hay, H. D. Vandervell and K. C. Waugh, *J. Catal.*, 1987, **103**, 79.

27 R. M. Dell, F. S. Stone and P. F. Tiley, *Trans. Faraday Soc.*, 1953, **49**, 195.

28 B. Bems, M. Schur, A. Dassenoy, H. Junkes, D. Herein and R. Schlögl, *Chem.–Eur. J.*, 2003, **9**, 2039.

29 I. Kasatkin, P. Kurr, B. Kniep, A. Trunschke and R. Schlögl, *Angew. Chem., Int. Ed.*, 2007, **46**, 7324.

30 C. O. Arean, J. S. D. Vinuela, J. M. R. Gonzalez and A. M. Arjona, *Mater. Chem.*, 1981, **6**, 165.

31 (*a*) G. Busca, U. Costantino, F. Marmottini, T. Montanari, P. Patrono, F. Pinzari and G. Ramis, *Appl. Catal., A*, 2006, **310**, 70; (*b*) Y. Tang, Y. Liu, P. Zhu, Q. Xue, L. Chen and Y. Lu, *AIChE J.*, 2009, **55**, 1217; (*c*) S. Velu, K. Suzuki, M. Okazaki, M. P. Kapoor, T. Osaki and F. Ohashi, *J. Catal.*, 2000, **194**, 373.

32 (*a*) X. Zhang, J. Huang, K. Ding, Y. Hou, X. Wang and X. Fu, *Environ. Sci. Technol.*, 2009, **43**, 5947; (*b*) N. Kumagai, L. Ni and H. Irie, *Chem. Commun.*, 2011, **47**, 1884.

33 M. M. Günter, T. Ressler, R. E. Jentoft and B. Bems, *J. Catal.*, 2001, **203**, 133.

34 M. V. Twigg and M. S. Spencer, *Top. Catal.*, 2003, **22**, 191.

35 K. Faungnawakij, T. Fukunaga, R. Kikuchi and K. Eguchi, *J. Catal.*, 2008, **256**, 37.

36 L. M. Plyasova, L. P. Solovyeva, T. A. Krieger, O. V. Makarova and T. M. Yurieva, *J. Mol. Catal. A: Chem.*, 1996, **105**, 61.

37 (*a*) W. Jochum, S. Penner, R. Kramer, K. Föttinger, G. Rupprechter and B. Klötzer, *J. Catal.*, 2008, **256**, 278; (*b*) W. Jochum, S. Penner, K. Föttinger, R. Kramer, G. Rupprechter and B. Klötzer, *J. Catal.*, 2008, **256**, 268.

38 M. S. Spencer, *Top. Catal.*, 1999, **8**, 259.

39 (*a*) N. Y. Topsoe and H. Topsoe, *Top. Catal.*, 1999, **8**, 267; (*b*) R. N. d'Alnoncourt, X. Xia, J. Strunk, E. Loffler, O. Hinrichsen and M. Muhler, *Phys. Chem. Chem. Phys.*, 2006, **8**, 1525; (*c*) J. D. Grunwaldt, A. M. Molenbroek, N. Y. Topsoe, H. Topsoe and B. S. Clausen, *J. Catal.*, 2000, **194**, 452.